Biosensors and Bioelectronics 139 (2019) 111312

Contents lists available at ScienceDirect

Biosensors and Bioelectronics

journal homepage: www.elsevier.com/locate/bios

Dual signal amplification photoelectrochemical biosensor for highly sensitive human epidermal growth factor receptor-2 detection

Xiaoxi Guo[a], Shuping Liu[b], Minghui Yang[b], Huitong Du[a], Fengli Qu[a,*]

[a] College of Chemistry and Chemical Engineering, Qufu Normal University, Qufu, 273165, Shandong, China
[b] College of Chemistry and Chemical Engineering, Central South University, Changsha, 410083, Hunan, China

ARTICLE INFO

Keywords:
Human epidermal growth factor receptor-2
WS_2 nanowire array
Photoelectrochemical biosensor
Dual signal amplification strategy
Localized surface plasmon resonance

ABSTRACT

Photoelectrochemical (PEC) biosensor for highly sensitive detection of breast cancer biomarker human epidermal growth factor receptor-2 (HER2) is reported utilizing a dual signal amplification strategy. The biosensor was prepared based on tungsten sulfide nanowire array on Ti mesh (WS_2 NW/TM). Such WS_2 NW/TM electrode can generate photoelectric signal under visible light excitation. The HER2 aptamer was wrapped onto the nanowire array surface for specific binding with HER2 molecules, and gold nanoparticles (Au NPs) that modified with glucose oxidase (GOx) and HER2 binding peptide was utilized for signal amplification. The H_2O_2 that generated by GOx catalyzed glucose reaction and localized surface plasmon resonance of Au NPs can both enhance the PEC current intensity of the biosensor, leading to dual signal amplification. The PEC current intensity is enhanced linearly with HER2 concentration in the 0.5–10 ng/mL range with limit of detection of 0.36 ng/mL. Such biosensor was applied for the detection of HER2 in breast cancer serum samples with detection results in good agreement with commercial ELISA results.

1. Introduction

Photoelectrochemistry is the technique that combines photochemical process and electrochemical technology (Fan et al., 2016; R. Yang et al., 2018; Chen et al., 2010). The modern photoelectrochemistry was basically launched in 1954 by Brattain and Garrett (Brattain et al., 1955). The photoelectrochemical (PEC) detection inherited the exciting advantages of electrochemistry, such as simple instrumentation, fast detection process, low cost and easy of miniaturization (Feng et al., 2017; Lu et al., 2006; Li et al., 2018; Q. Yang et al., 2018; Shen et al., 2018). In addition, since the excitation source and detection signal are different, PEC detection has low background signal and high sensitivity. As a result, PEC detection has found wide applications for detection of various analytes, such as protein biomarkers, DNA, metal ions, small molecules and so on (Zhang et al., 2018; Zhao et al., 2018; Lu et al., 2008; Shi et al., 2018).

Photoactive materials significantly affect the analytical performances of PEC sensors (Hu et al., 2018). In recent years, different materials have been studied, with the most widely reported are inorganic semiconductor nanomaterials or quantum dots (Zhao et al., 2015a,b; Chen et al., 2008; Chang et al., 2010). Significant efforts have also been tried for the development of composite materials to increase the efficient utilization of solar light and enhance the PEC efficiency. For example, TiO_2 was combined with quantum dots to broaden the absorption of solar light and amplify the photocurrent response (Zhao et al., 2015a,b). Tungsten sulfide (WS_2), a good PEC material has been widely investigated in the field of energy storage and catalysis because of broadband light absorption, remarkable carrier mobility and ease of functionalization. WS_2 nanowire array on Ti mesh (WS_2 NW/TM), as a three dimension electrode, has large surface area, high active sites density, low series resistance, marvelous stability and beneficial diffusion of electrolyte (Guo et al., 2018a,b; Guo et al., 2018a,b; Zhang et al., 2017), which is beneficial for generating photoelectric signal.

Human epidermal growth factor receptor-2 (HER2) is a biomarker of breast cancer that overexpressed in around 20–30% of breast cancer tumors (Shen et al., 2017; Hu et al., 2017; Peng et al., 2018). In this paper, we developed a novel PEC biosensor for HER2 detection based on WS_2 NW/TM as photoactive material and a dual signal amplification strategy. Such WS_2 NW/TM electrode synthesized by a facile hydrothermal sulfide method can generate photoelectric signal under visible light excitation. Gold nanoparticles (Au NPs) modified with glucose oxidase (GOx) and HER2 specific peptide (Li et al., 2018) were utilized for signal amplification. Such bioconjugates can be captured by the HER2 aptamer (Hu et al., 2017) wrapped nanowire array. The GOx can catalyze glucose to produce H_2O_2, which as a sacrificial electron donor can scavenge the holes generated on the valence band of WS_2 NW/TM

* Corresponding author.
E-mail address: fengliquhn@hotmail.com (F. Qu).

https://doi.org/10.1016/j.bios.2019.05.017
Received 20 February 2019; Received in revised form 4 May 2019; Accepted 6 May 2019
Available online 10 May 2019
0956-5663/

(An et al., 2010; Zirak et al., 2015), and thus amplifies the PEC signal. In addition, the introducing of the localized surface plasmon resonance (LSPR) of Au NPs into PEC system can also enhance photoelectric transfer efficiency and increase the photocurrent response as well (Z. Yan et al., 2016; Yan et al., 2016; Zhao et al., 2011;Cushing et al., 2012; You et al., 2012). In such system, dual signal amplification was achieved, leading to high sensitivity of the sensor. The reported signal amplification method can be adapted to other PEC sensors and has a great potential for clinical and biological analysis.

2. Experimental section

2.1. Materials and reagents

The peptide specific to HER2 (CKLRLEWNR) was purchased from GL Biochem Ltd. (Shanghai, China). The HER2 specific DNA aptamer (5′-GCA GCG GTG TGG GG-3′) was obtained from Sangon Biotech Co., Ltd. (Shanghai, China). The human HER2 proteins were acquired from Abcam Co., Ltd. (Cambridge, MA, USA). Bovine serum albumin (BSA), glucose oxidase and $HAuCl_4{\cdot}2H_2O$ were bought from Sigma-Aldrich (St. Louis, MO). $Na_2WO_4{\cdot}2H_2O$, HCl, Na_2HPO_4, NaH_2PO_4, $H_2C_2O_4{\cdot}2H_2O$, $(NH_4)_2SO_4$, thiocarbamide, $Na_3C_6H_5O_7{\cdot}2H_2O$ and glucose were purchased from Aladdin Ltd. (Shanghai, China). The human HER2 ELISA kit was purchased from Jining Biotech Co., Ltd. (Shanghai, China). Human serum samples were gathered from the Second Xiangya hospital. All experiments were carried out in accordance with the guidelines of the National Institute of Health, China, and approved by the Institutional Ethical Committee (IEC) of Central South University. We also obtained informed consent for any experimentation with human serum samples. All stock solutions were prepared with deionized water. All reagents were used as received.

2.2. Synthesis of WS_2 NW/TM electrodes

The WS_2 NW/TM was prepared by a simple hydrothermal sulfide method. 5 mmol $Na_2WO_4{\cdot}2H_2O$ was dissolved in 40 mL deionized water. Subsequently, 3 M HCl was added by drop until the pH of solution attained 1.2 and the solution turned pale yellow. After that, 14 mmol $H_2C_2O_4{\cdot}2H_2O$ was added into aforementioned mixture and diluted to 100 mL, and the H_2WO_4 precursor was formed. Then, 5 g $(NH_4)_2SO_4$ and 10.8 mmol thiocarbamide were dissolved in precursor successively. The solution was transferred to 50 mL Teflon-lined stainless autoclave. A piece of Ti mesh (2 cm × 4 cm) that was carefully pretreated by hydrochloric acid, ethanol and deionized water in turn, was put into the autoclave, sealed, and maintained at 180 °C for 16 h. When the autoclave cooled to room temperature, the Ti mesh was taken out and washed by deionized water for several times and dried at 60 °C for 12 h. The as-obtained sample was finally calcined in N_2 atmosphere at 600 °C for 2 h.

2.3. Preparation of [GOx-Au NPs-peptide] bioconjugates

The Au NPs were synthesis according to a reported method (Li et al., 2018). After the 100 mL deionized water containing 0.001% $HAuCl_4{\cdot}2H_2O$ was heated to boiling, 2% $Na_3C_6H_5O_7{\cdot}2H_2O$ (w/v) was added, and then the mixture was refluxed for 15 min and stirred to ambient temperature. To prepare the GOx-Au NP-peptide bioconjugates, GOx (50 μL, 0.4 mg/mL) and the HER2 specificity peptide (50 μL, 0.4 mg/mL) were added to 2 mL Au NPs solution. The mixture was gently vibrated for 12 h. The as-obtained solution was centrifuged and re-dispersed into 2 mL of deionized water.

2.4. Biosensor fabrication

The WS_2 NW/TM (0.5 cm × 0.5 cm) was immersed in 5 μM aptamer solution for 4 h. Next, the electrode was blocked by 1% BSA for 30 min at 4 °C. Then, the resulting electrode was washed by deionized water and different concentration of HER2 was spread onto it for 2 h at 4 °C. Finally, the 40 μL as-prepared GOx-Au NP-peptide bioconjugates were drop on the surface of the electrode for 2 h. The assembled electrode was incubated in 7 mL PBS (0.1 M, pH = 7.0) containing 10 mM glucose for 25 min at 37 °C, followed by the respective PEC measurements. All tests were performed at 0 V vs. SCE.

2.5. Characterization methods

All the electrochemical measurements were performed by a CHI 650D electrochemical workstation (CH Instruments, Inc., Shanghai) in a typical three electrode configuration, utilizing WS_2 NW/TM (0.5 cm × 0.5 cm) as working electrode, a saturated calomel electrode (SCE) as reference electrode and a platinum wire as auxiliary electrode. The human HER2 ELISA was conducted on an ELX800 microplate reader (BioTek). Powder X-ray diffraction (XRD) patterns were acquired on a LabX XRD-6100 X-ray diffractometer with Cu Kα radiation (40 kV, 30 mA) of wavelength 0.154 nm (SHIMADZU, Japan). Scanning electron microscopy (SEM) measurements were performed on a tungsten lamp-equipped SU3500 scanning electron microscope at an accelerating voltage of 20 kV (HITACHI, Japan). Transmission electron microscopy (TEM) measurements were conducted on a Hitachi H-8100 electron microscopy (Hitachi, Tokyo, Japan) at an accelerating voltage of 200 kV. X-ray photoelectron spectroscopy (XPS) measurements were carried out on an ESCALABMK II X-ray photoelectron spectrometer using Mg as the exciting source. The excitation source of homogeneous light (420 nm) was filtered from the xenon lamp (PLS-SXE300D, China). UV–vis absorbance measurement was performed on Shimadzu UV-2450 spectrophotometer.

3. Results and discussion

3.1. Characterization of WS_2 NW/TM and gold nanoparticles

Fig. 1A depicts the X-ray diffraction (XRD) patterns of WS_2 NW/TM and bare Ti mesh. The WS_2 diffraction peaks located at 13.7°, 33.8°, 39.8°, 49.6°, 55.4°, 59.8°, 60.9° and 61.8° are indexed to the (002), (101), (103), (105), (106), (008), (112) and (007) planes (JCPDS No. 08–0237), respectively (Wu et al., 2012; Lim et al., 2017). And the peaks at 41.3°, 70.5° and 76° are derived from Ti mesh (JCPDS No 44–1294) (Ren et al., 2017). In addition, the broad peak at around 23.6° is attributed to WO_3 which may stem from surface oxidation of material or contamination (Cai et al., 2015). Fig. 1B and C displays the scanning electron microscopy (SEM) images of WS_2 NW/TM. As observed, the WS_2 is in the morphology of nanowire array and the smooth surface of Ti mesh (Fig. S1) was completely covered by the WS_2 nanowires. Furthermore, the nanowire morphology was investigated by transmission electron microscopic (TEM) (Fig. 1D). The high-resolution transmission electron microscopy (HRTEM) (Fig. 1E) taken from the single nanowire exhibits well-resolved interplanar spacing which were determined to be 0.61 nm indexed to (002) plane. Moreover, the TEM image of Au NPs is shown in Fig. 1F. The Au NPs appear as quasi-spherical particles with the size ca. 17 nm. And the UV–vis absorption peak of Au NPs is seen at around 520 nm (Fig. S2A), which indicates the successful formation of Au NPs (Hu et al., 2007; Zhang et al., 2015). Moreover, the dynamic light scattering spectrum (Fig. S2B) demonstrates the as-made Au NPs are uniform in size. In the meantime, the X-ray photoelectron spectroscope (XPS) analysis was employed to identify the element valence state and examine chemical composition of material. As shown in Fig. 1G, the binding energies located at 32.1 and 34.2 eV were assigned to W $4f_{7/2}$ and W $4f_{5/2}$, respectively, which indicated the presence of W^{4+} (Pu et al., 2014; Akple et al., 2015). Fig. 1H depicts the high-resolution XPS spectrum of S 2p and the peaks at the binding energies of 163.2 and 164.4 eV corresponded to S^{2-} state (Zhong et al., 2016). The strong peak located at 168.9 eV resulted from oxygen containing sulfur species

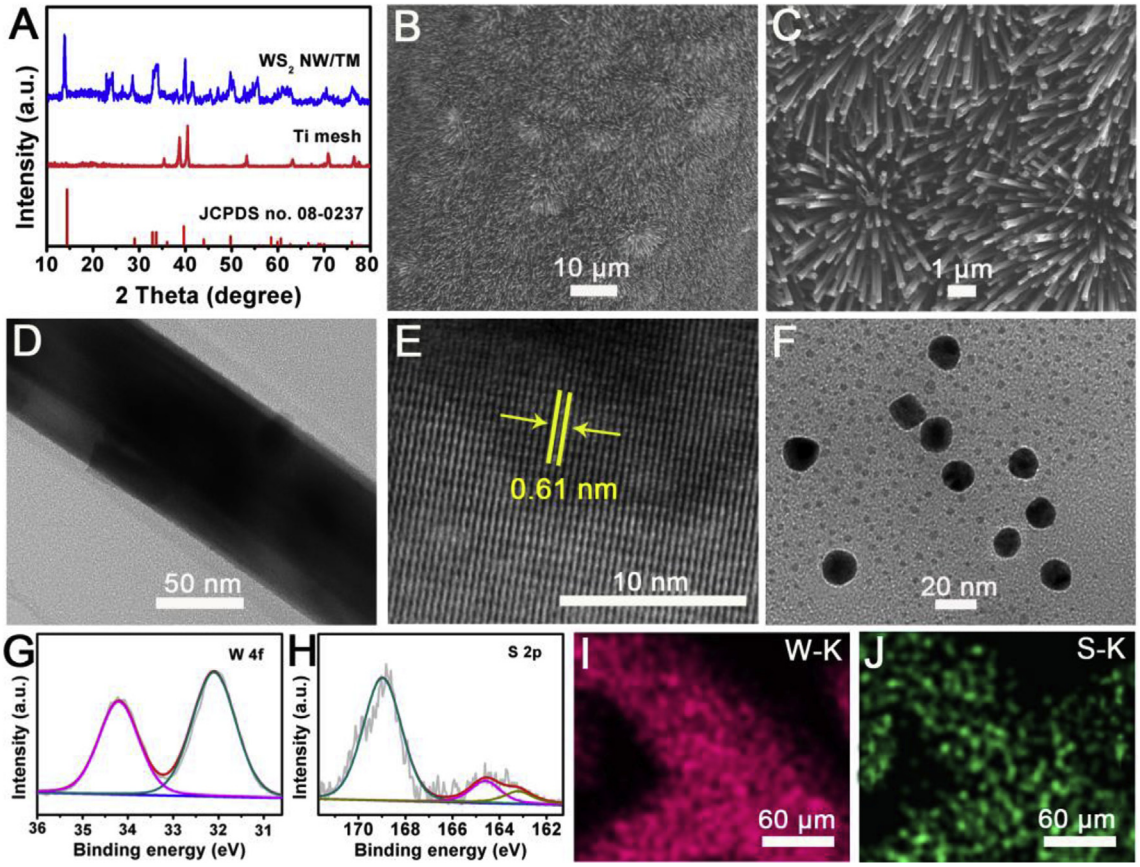

Fig. 1. (A) XRD patterns of WS_2 NW/TM and bare Ti mesh. (B) and (C) SEM images for WS_2 NW/TM. (D) TEM image and (E) HRTEM image of WS_2 nanowire. (F) TEM image of Au NPs. XPS spectra of WS_2 NW/TM in (G) W 4f and (H) S 2s regions. EDX elemental mapping images of (I) W and (J) S elements for WS_2 NW/TM.

(Escuderol et al., 2016; Du et al., 2018). The energy dispersive X-ray (EDX) mapping images imply the W and S elements evenly distributed over WS_2 NW/TM (Fig. 1I and J).

3.2. Electrochemical impedance spectroscopy (EIS) characterization of the sensor modification process

After characterization of the WS_2 NW, the WS_2 NW/TM was utilized to prepare the PEC sensor. It is well-known that EIS is a convenient and effective approach to characterize the surface features of modified electrodes and monitor the progressive construction of biosensor (Chen et al., 2017). The charge transfer resistances (R_{ct}) of different modified electrodes are evaluated by the semicircle diameter of Nyquist plots. And the R_{ct} is estimated by the semicircle diameter. As shown in Fig. 2, the Nyquist plots for WS_2 NW/TM, WS_2 NW/TM-aptamer, WS_2 NW/TM-aptamer-BSA, WS_2 NW/TM-aptamer-BSA-HER2, WS_2 NW/TM-aptamer-HER2-[peptide-Au-GOx] were test in phosphate buffer solution (PBS; 0.1 mM, pH = 7.0) containing 5 mM $[Fe(CN)_6]^{3-/4-}$. The WS_2 NW/TM possesses the lowest R_{ct} value (curve a). As the electrode was modified by aptamer, BSA, HER2 and bioconjugates step by step, the R_{ct} values of the electrode was increased, which may be attributed to the modified substance hindering the access of the redox probe ($[Fe(CN)_6]^{3-}$/$[Fe(CN)_6]^{4-}$) to the electrode surface. These results indicate successful assembly of biomolecule on the surface of the electrode.

3.3. Photoelectrochemical response of biosensor for HER2 detection

Scheme A shows the schematic representation for the synthesis of the Au NPs signal probe and the preparation of the biosensor. In the presence of visible light irradiation, the photon energy collected by WS_2 NW/TM was higher than that of its band gap, which led to the electron

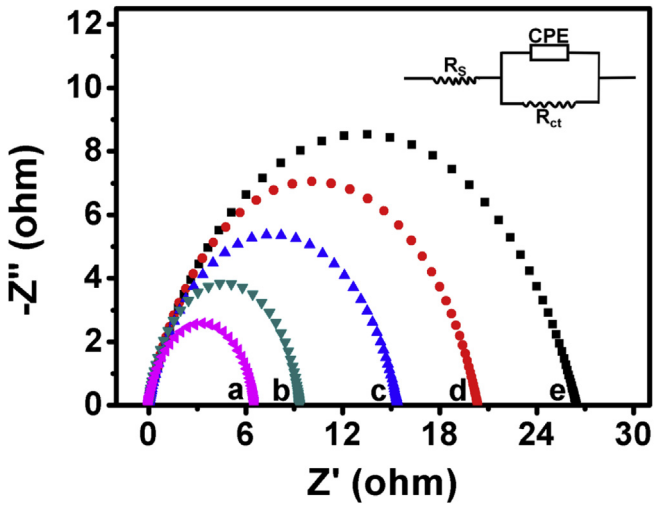

Fig. 2. Nyquist plots of EIS for different modified electrodes: (a) WS_2 NW/TM, (b) WS_2 NW/TM-aptamer, (c) WS_2 NW/TM-aptamer-BSA, (d) WS_2 NW/TM-aptamer-BSA-HER2, (e) WS_2 NW/TM-aptamer-HER2-[peptide-Au NPs-GOx].

transfer from valence band (VB) to conduction band (CB), generating electron-hole (e^--h^+) pair (Scheme B). Then the CB electron was transferred to the surface of Ti mesh and the hole was scavenged by H_2O_2, which resulted in photocurrent. Moreover, the LSPR of Au NPs generated a collective oscillation of free electrons, which made the hot electrons transferred from Au to the CB of the WS_2 NW/TM directly, thus further enhancing the photoelectric transfer efficiency. In order to confirm mechanism of sensing, PEC responses of different modified

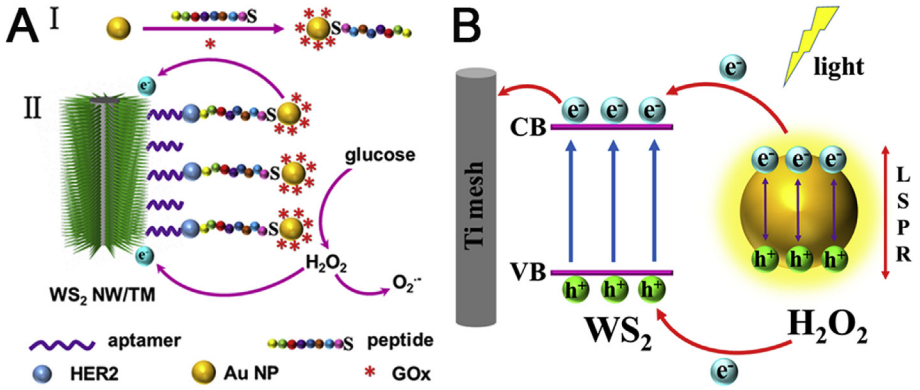

Scheme 1. (A) Schematic diagram of the process to synthesize the Au NP signal probe and fabricate PEC sensor for HER2 detection. (B) Schematic mechanism of the operating PEC system.

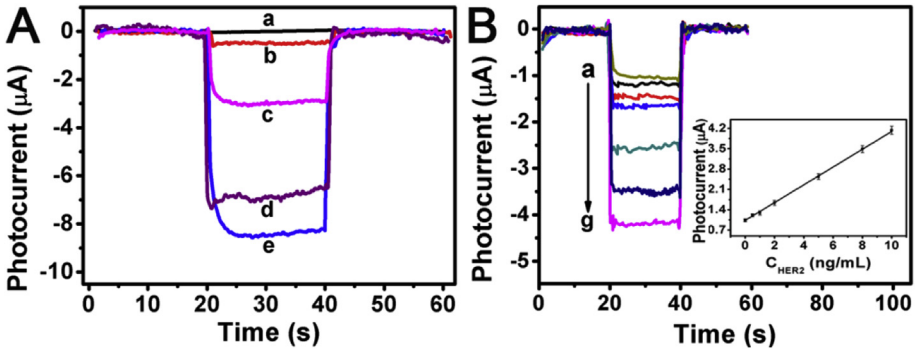

Fig. 3. (A) PEC responses of (a) bare Ti mesh, (b) WS_2 NW/TM, (c) WS_2 NW/TM-Au NPs, (d) WS_2 NW/TM containing 5 mM H_2O_2, (e) WS_2 NW/TM-Au NPs containing 5 mM H_2O_2 in 0.1 M PBS (pH = 7.0). (B) Photoelectrochemical response of WS_2 NW/TM-aptamer-HER2-[peptide-Au-GOx] toward HER2 at different concentrations: (a) 0, (b) 0.5, (c) 1, (d) 2, (e) 5, (f) 8, (g) 10 ng/mL recorded in 0.1 M PBS containing 10 mM glucose. The inset is the linger range from 0.5 to 10 ng/mL for HER2 detection.

electrodes were studied (Fig. 3A). The bare Ti mesh substrate has no PEC signal after visible light irritation (curve a). The substrate displays a weak photocurrent response after being covered by WS_2 nanowire array (curve b), a narrow band gap semiconductor. It can be seen that the photoelectrochemical current intensity is significantly enhanced obviously after addition of 5 mM H_2O_2 (curve d). Furthermore, the WS_2 NW/TM modified by Au NPs shows a strong photoelectric signal, which attributed to the improved light absorption properties and conductivity (curve c). Most importantly, when 5 mM H_2O_2 was added, the photocurrent response enhanced more than about 3 times (curve e). It is striking to note that H_2O_2 as a sacrificial electron donor can scavenge the holes generated on the valence band of WS_2 NW/TM, hence boosts the photocurrent signal. Meanwhile, the addition of Au NPs into electrolyte can also leads to enhanced photocurrent response.

Fig. 3B depicts the photoelectric changes of biosensor in the present of different concentrations of HER2. As the HER2 concentrations increased from 0 to 10 ng/mL, the photocurrent increased accordingly. Each concentration sample was repeated for 6 times. The inset exhibits a good linear relationship between the change of photocurrent and the HER2 concentration, with a linear correlation coefficient of 0.998. Moreover, on the basis of S/N = 3, the calculated limit of detection is 0.36 ng/mL, which is compared favorable to other reported literature for HER2 detection (Table S1). The increase of photocurrent in the presence of HER2 is ascribed to GOx on Au NPs that catalyzed glucose reaction to produce H_2O_2. In addition, the Au NPs itself can also enhance the photocurrent response. In such sandwich type assay, the time of glucose oxidase catalyzing glucose to product H_2O_2 affect the performance of the sensor. Fig. S3 shows the effect of the GOx catalytic reaction time on the photoelectric response in the range from 0 to 35 min. The photocurrent response enhanced with increase of catalytic time and then reached a plateau at 25 min. Thus, subsequent experiments employed 25 min as the optimum time for all the catalytic glucose steps of the assay.

3.4. Biosensor selectivity, reproducibility stability

Practical serum samples are complicated and some coexisting proteins in human serum may interfere HER2 detection. In order to achieve precise detection of HER2 in real sample, good selectivity of the sensor is of great importance. As shown in Fig. 4, the 1 ng/mL concomitant proteins such as β-site amyloid precursor protein cleaving enzyme 1 (BACE1), carcinoembryonic antigen (CEA), human immunoglobulin G (human IgG), human immunoglobulin M (human IgM), P53, protein kinase A (PKA) and were measure at the concentration of 1 ng/mL for 6 times. The aforementioned interferential proteins exhibit relative weak photocurrent responses compared to those of HER2. In this sense, the

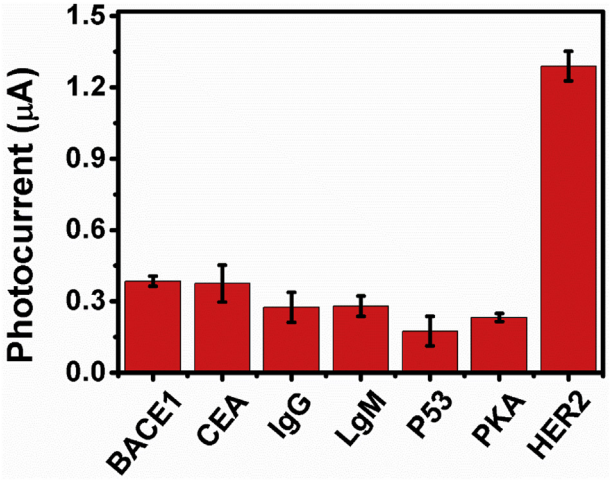

Fig. 4. Selectivity of proposed biosensor to HER2 (1 ng/mL) by comparing it to the interferential proteins at the concentration of 1 ng/mL, BACE1, CEA, IgG, LgM, P53, PKA.

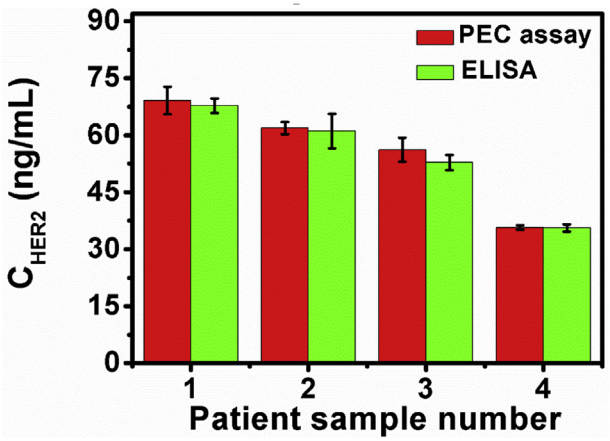

Fig. 5. Comparison of the biosensor with the ELISA for HER2 detection in human serums.

fabricated biosensor can specifically identify HER2, and thus possesses good selectivity.

Reproducibility of the fabricated biosensor was investigated by analyzing three concentrations of HER2 samples in triplicate. The recovery test was conducted by standard addition method. As observed in Table S2, the recoveries were 108.2%, 98.6% and 101.3% at 0.5, 5 and 10 ng/mL of HER2, respectively. And the relative standard deviation (RSD) of the sensor measuring results were 1.5%, 2.3% and 3.2%, correspondingly, implying the experimental results are highly reliable. Besides, the stability of biosensor was assessed by chronopotentiometric measurement. The biosensor was test for more than 600 s and repeated the illumination process for more than 15 times. After long-time measurement, the photocurrent had no obvious decreased (Fig. S4), suggesting good stability.

3.5. Measurement of HER2 in breast cancer patients' serum

High selectivity and superb reproducibility and stability of the biosensor were verified by the above results. It is necessary to evaluate the potential clinical applicability of such biosensor for HER2 detection in real samples. The four human serum samples from breast cancer patients were diluted 1000 times with 0.1 M PBS (pH = 7.0) and stored at −20 °C for HER2 detection. Then, these samples were analyzed by the proposed biosensor for 6 times. The testing results were compared with those obtained from commercial ELISA assay. As observed in Fig. 5, there was no remarkable difference in HER2 detection results between the two approaches, which indicated the designed sandwich biosensor has great potential as a reliable strategy for HER2 detection in serum sample.

4. Conclusion

In summary, a novel PEC biosensor was prepared for sensitive detection of HER2 utilizing a dual signal amplification method. H_2O_2, as a sacrificial electron donor, scavenges the holes generated on the valence band of WS_2, resulting in amplification of photocurrent response. Furthermore, the LSPR of Au NPs was introduced to enhance photoelectric transfer efficiency, which increased the PEC signal as well. Accordingly, the dual signal amplification biosensor was qualified to sensitive detection HER2 with a limit detection as low as 0.36 ng/mL and exhibited high selectivity and good stability. Such fabricated biosensor sheds light on a new methodology for PEC detection, and has a great potential for clinical and biological analysis in the future.

5. Declaration of interest statement

We declare that we have no financial and personal relationships with other people or organizations that can inappropriately influence our work, there is no professional or other personal interest of any nature or kind in any product, service and/or company that could be construed as influencing the position presented in, or the review of, the manuscript entitled.

CRediT authorship contribution statement

Xiaoxi Guo: Conceptualization, Validation, Data curation, Formal analysis, Writing - original draft. **Shuping Liu:** Formal analysis, Data curation. **Minghui Yang:** Conceptualization, Supervision, Writing - review & editing. **Huitong Du:** Formal analysis, Data curation. **Fengli Qu:** Funding acquisition, Supervision, Writing - review & editing.

Acknowledgment

This work was supported by the National Natural Science Foundation of China (No. 21775089), the Outstanding Youth Foundation of Shandong Province (No. ZR2017JL010), and the Key Research and Development Program of Jining City (2018ZDGH032).

Appendix A. Supplementary data

Supplementary data to this article can be found online at https://doi.org/10.1016/j.bios.2019.05.017.

References

Akple, M.S., Low, J., Wagehb, S., Al-Ghamdi, A.A., Yu, J., Zhang, J., 2015. Appl. Surf. Sci. 358, 196–203.
An, Y., Tang, L., Jiang, X., Chen, H., Yang, M., Jin, L., Zhang, S., Wang, C., Zhang, Wen, 2010. Chem. Eur J. 16, 14439–14446.
Brattain, W.H., Garrett, C.G.B., 1955. Bell Syst. Tech. J 34, 129–136.
Cai, Z., Li, H., Yang, X., Guo, X., 2015. Sensor. Actuator. B Chem. 219, 346–353.
Chang, H., Zhang, H., Lv, X., Li, J., 2010. Electrochem. Commun. 12, 483–487.
Chen, J., Zhao, G.C., 2017. Biosens. Bioelectron. 98, 155–160.
Chen, D., Zhang, H., Hu, S., Li, J., 2008. J. Phys. Chem. C 112, 117–122.
Chen, D., Zhang, H., Li, X., Li, J., 2010. Anal. Chem. 82, 2253–2261.
Cushing, S.K., Li, J., Meng, F., Senty, T.R., Suri, S., Zhi, M., Li, M., Bristow, A.D., Wu, N., 2012. J. Am. Chem. Soc. 134, 15033–15041.
Du, H., Kong, R., Qu, F., Lu, L., 2018. Chem. Commun. 54, 10100–10103.
Escudero1, M.J., Fuerte, A., 2016. Fuel Cells 3, 340–348.
Fan, G.C., Shi, X.M., Zhang, J.R., Zhu, J.J., 2016. Anal. Chem. 88, 10352–10356.
Feng, K., Yang, M., Xie, F., Diao, G., Ou, M., Huang, H., 2017. Anal. Methods 9, 6754–6759.
Guo, X., Kong, R.M., Zhang, X., Du, H., Qu, F., 2018a. ACS Catal. 8, 651–655.
Guo, X., Zhu, S., Kong, R.M., Zhang, X., Qu, F., 2018b. ACS Sustain. Chem. Eng. 6, 1545–1549.
Hu, J., Wang, Z., Li, J., 2007. Sensors 7, 3299–3311.
Hu, L., Hu, S., Guo, L., Shen, C., Yang, M., Rasooly, A., 2017. Anal. Chem. 89, 2547–2552.
Hu, T., Zheng, Y.N., Li, M.J., Liang, W.B., Chai, Y.Q., Yuan, R., 2018. Anal. Chem. 90, 6096–6101.
Li, X., Shen, C., Yang, M., Rasooly, A., 2018. Anal. Chem. 90, 4764–4769.
Lim, Y.V., Wang, Y., Kong, D., Guo, L., Wong, J.I., Anga, L.K., Yang, H.Y., 2017. J. Mater. Chem. 5, 10406–10415.
Lu, W., Wang, G., Jin, Y., Yao, X., Hu, J., Li, J., 2006. Appl. Phys. Lett. 89, 263902.
Lu, W., Jin, Y., Wang, G., Chen, D., Li, J., 2008. Biosens. Bioelectron. 23, 1534–1539.
Peng, Z., Lu, J., Zhang, L., Liu, J., Li, J., 2018. Analyst 143, 5264–5270.
Pu, Z., Liu, Q., Asiri, A.M., Obaid, A.Y., Sun, X., 2014. Electrochim. Acta 134, 8–12.
Ren, X., Ge, R., Zhang, Y., Liu, D., Wu, D., Sun, X., Du, B., Wei, Q., 2017. J. Mater. Chem. 5, 7291–7294.
Shen, C., Zeng, K., Luo, J., Li, X., Yang, M., Rasooly, A., 2017. Anal. Chem. 89, 10264–10269.
Shen, C., Liu, S., Li, X., Zhao, Dan, Yang, M., 2018. Microchim. Acta 185, 547.
Shi, X.M., Mei, L.P., Zhang, N., Zhao, W.W., Xu, J.J., Chen, H.Y., 2018. Anal. Chem. 90, 8300–8303.
Wu, Z., Fang, B., Bonakdarpour, A., Sun, A., Wilkinson, D.P., Wang, D., 2012. Appl. Catal. B Environ. 125, 59–66.
Yan, Z., Wang, Z., Miao, Z., Liu, Y., 2016. Anal. Chem. 88, 922–929.
Yan, R., Bao, J., Tu, W., Dai, Z., 2016. Chem. Commun. 52, 11799–11802.
Yang, R., Zou, K., Li, Y., Meng, L., Zhang, X., Chen, J., 2018. Anal. Chem. 90, 9480–9486.
Yang, Q., Hao, Q., Lei, J., Ju, H., 2018. Anal. Chem. 90, 3703–3707.
You, H., Shi, W., Li, J., Guo, L., 2012. J. Phys. Chem. C 116, 6490–6494.

Zhang, J., Li, C., Zhang, X., Huo, S., Jin, S., An, F., Wang, X., Xue, X., Okeke, C.I., Duan, G., Guo, F., Zhang, X., Hao, J., Wang, P.C., Zhang, J., Liang, X., 2015. Biomaterials 42, 103–111.
Zhang, X., Si, C., Guo, X., Kong, R., Qu, F., 2017. J. Mater. Chem. 5, 17211–17215.
Zhang, N., Ruan, Y.F., Zhang, L.B., Zhao, W.W., Xu, J.J., Chen, H.Y., 2018. Anal. Chem. 90, 2341–2347.
Zhao, W.W., Wang, J., Xu, J.J., Chen, H.Y., 2011. Chem. Commun. 47, 10990–10992.
Zhao, W.W., Wang, J., Zhu, Y.C., Xu, J.J., Chen, H.Y., 2015a. Anal. Chem. 87, 9520–9531.
Zhao, W.W., Xu, J.J., Chen, H.Y., 2015b. Chem. Soc. Rev. 44, 729–741.
Zhao, W.W., Xu, J.J., Chen, H.Y., 2018. Anal. Chem. 90, 615–627.
Zhong, Y., Zhao, G., Ma, F., Wu, Y., Hao, X., 2016. Appl. Catal. B Environ. 199, 466–472.
Zirak, M., Zhao, M., Moradlou, O., Samadi, M., Sarikhani, N., Wang, Q., Zhang, H.L., Moshfegh, A.Z., 2015. Sol. Energy Mater. Sol. Cells 141, 260–269.